Available online at www.sciencedirect.com
SCIENCE DIRECT
Optics & Laser Technology 37 (2005) 271–280
Optics & Laser Technology
www.elsevier.com/locate/optlastec

Projection ablation of glass-based single and arrayed microstructures using excimer laser

Ying-Tung Chen[a], Kung-Jeng Ma[b], Ampere A. Tseng[c,*], P.H. Chen[c]

[a] Department of Mechanical Engineering, Chung Cheng Institute of Technology, Tashi 33508, Taiwan
[b] Department of Mechanical Engineering, Chung Hua University, Hsinchu 30067, Taiwan
[c] Department of Mechanical Engineering, National Taiwan University, Taipei 10617, Taiwan

Received 7 February 2004; received in revised form 17 April 2004; accepted 17 April 2004

Available online 15 June 2004

Abstract

Ablation of single and arrayed microstructures using an excimer laser is studied. The single feature microstructures are fabricated for evaluating the ablation mechanism, threshold fluence, and associated material removing (ablation) rate. The morphology changes during ablation are investigated with the focus on the formation of the ablation defects, debris or recast. The possibility of removing these defects is also evaluated and demonstrated. The present study concentrates on the borosilicate glass, although ablation of polyimide and silicon are performed and discussed for comparison. Polyimide and silicon are the most popular polymer or semiconductor material used in the electronics industry. The arrayed microstructures are ablated to demonstrate the fact that, by repetition of a simple-patterned mask associated with synchronized laser pulses and substrate movement, arrayed and more complex structures can be cost-effectively manufactured. The potential applications of these arrayed microstructures are discussed and illustrated. A low-cost replication technique that uses the arrayed microstructure presently machined as the forming mold for making electroforming nickel microneedles is specifically presented. Finally, the potential areas of using excimer laser in micromachining of glass-based structures for future research are also briefly covered.
© 2004 Elsevier Ltd. All rights reserved.

Keywords: Ablation; Ablation rate; Arrayed microstructure; Debris; Excimer laser; Glass; Micromachining; Microneedle; Morphology; Polyimide; Silicon

1. Introduction

Excimer lasers possess ultraviolet (UV) wavelength with comparatively short pulse duration to ensure high peak densities (fluences) and high pulse energies, which allow the radiation to be efficiently absorbed by the surfaces of most materials. Excimer lasers remove materials from the substrates through the ablation mechanism, by either vaporization (photothermal) or decomposition (photochemical) or by a combination of these two. The excimer laser has been one of the most capable and popular tools for machining microstructures with feature sizes on the order of 1–100 μm for all kinds of materials, including polymers, metals, and ceramics [1–3].

Recently, excimer lasers are increasingly used for machining glass-based materials, because they are becoming the material of choice in photonics and communications industries as well as the emerging microelectromechanical system (MEMS) industry [4–7]. In general, the glass-based materials are extremely brittle and very difficult to be handled by traditional machining processes. As a result, the current major obstacle in preventing glass from meeting the industrial demands for miniaturization is that no sufficient microfabrication knowledge is available [8,9]. Therefore, the focus of the present study is to develop a cost effective laser ablation technique for creating glass-based microstructures and to understand the associated ablation phenomena, including the mechanism of laser/material interaction, threshold energy intensity, and

*Corresponding author. Department of Mechanical and Aerospace Engineering, Arizona State University, Box 876106, Tempe, AZ 85287-6106, USA. Tel.: +1-480-965-8201; fax: +1-480-965-1384.
E-mail address: ampere.tseng@asu.edu (A.A. Tseng).

0030-3992/$ - see front matter © 2004 Elsevier Ltd. All rights reserved.
doi:10.1016/j.optlastec.2004.04.007

ablation rate as well as the morphology and defect formation of the ablated microstructures.

A laser projection system using an Argon–Fluorine (ArF) excimer laser is adopted for the present ablation experiment. By machining simple microstructures, the morphology changes and debris formation during ablation are first studied. The possibility of removing these debris are then presented and demonstrated. The process efficiency, especially the impact of changing major operating parameters, such as the pulse fluence, pulse repetition rate, and pulse number, on the resulting microstructural shapes is also evaluated and discussed. The threshold fluence and the ablation rate are specifically established. One of the widely used optical glass, Schott SF-11 borosilicate glass, is chosen for the present study. To compare the ablation phenomena of glass, two of the most popular polymer and semiconductor materials used in the electronic industry, polyimide and silicon, are also fabricated at similar ablation conditions. A cost-effective scheme of using only a simple-shaped mask, also known as 'simple motif' mask, is developed for machining an assortment of arrayed microstructures. The replication technique for making electroformed nickel microneedles by using the laser machined glass-based array as the forming mold is specifically presented. The other applications of these arrayed structures are also discussed. Finally, recommendations for future efforts and trends are presented.

2. Experiment set-up

The projection micromachining is used in the present study. The main reason to use the projection writing scheme is to have a better control on the beam size. In this writing scheme, parallel laser beams are generated to illuminate a mask, whose demagnified image is then focused on the substrate. Excimer beams typically have broad spatial profiles and less desirable defined mode structure. Sometimes, it is difficult to obtain a sharp focused beam which is required in direct writing scheme in making precision microstructures. The workstation used consists of an ArF excimer laser source, an optical lens set, a moving stage, a mask holder, an optical table, and an outer protective shielding as shown in Fig. 1 [10]. The ArF laser manufactured by Lambda Physik (Germany) has a wavelength of 193 nm. A 7×7 fixed-array homogenizer is used to produce a 12×23 mm uniform illumination at the mask. The homogenizer is made by MicroLas (Germany), providing up to 60% transmission rate for the laser light, and it transforms the spatial non-uniform laser beam to an uniform overlapped beam. Projection lenses of various magnifications are used to transfer the pattern on the mask to the target, which is mounted on a high-precision piezoelectric x–y stage.

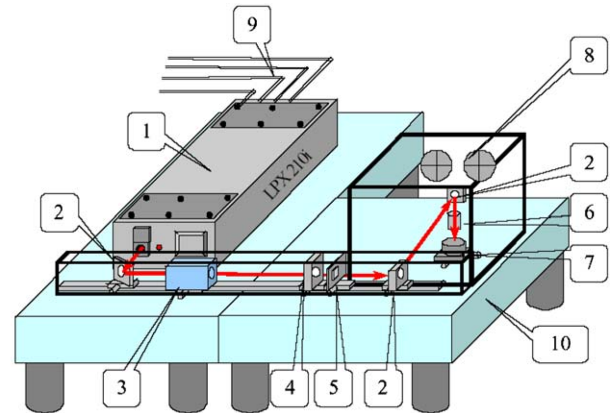

Fig. 1. ArF excimer laser micromachining workstation: (1) laser source (2) 45° mirror (3) homogenizer (4) condenser lens (5) mask (6) focus lens (7) moving stage (8) air conditioner (9) laser gas (10) optical table.

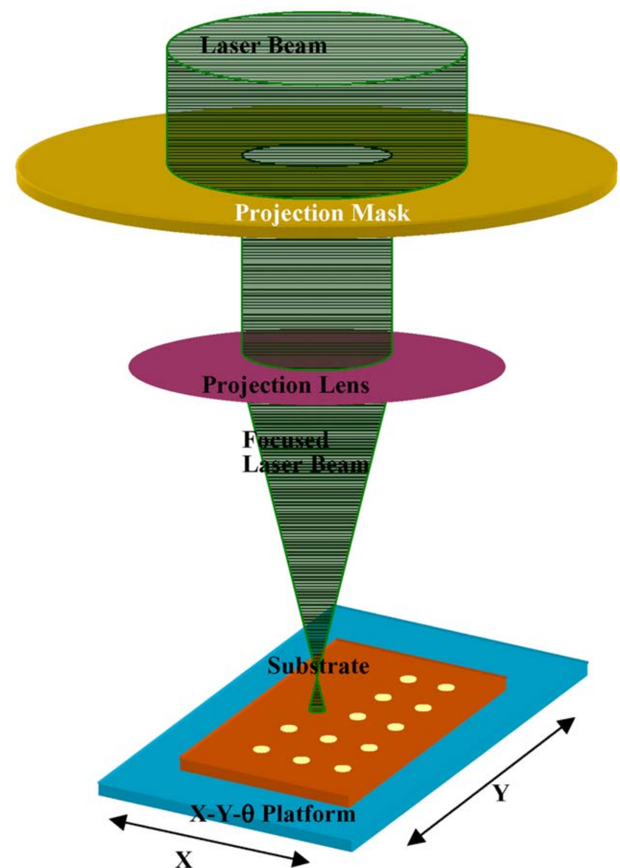

Fig. 2. Schematic of laser machining of arrayed microstructures.

The projection mask, having a single circular opening, is used to make the arrayed microstructures. The masks are 200 μm thick and are made of 304 stainless steel. The circular opening is chemically etched with a diameter of 200 μm. The projection lens used is the excimer laser focusing lens provided by CVI and it has a 74-mm focal length. As schematically explained in Fig. 2, the

projection system has been set to have a 10x demagnification and the sample is placed 1.4 mm away from the focal point or 75.4 mm from the projection lens. As a result, the circle printed onto the target or substrate is expected to be 20 μm in bore diameter. The main reason in selecting the 20 μm feature size, i.e., the circular opening diameter, in the present study is that any feature size on the order of 20 μm is beyond the normal feasible sizes of traditional drilling and shaping processes. Certainly, if the feature size is not 20 μm, the size of either the mask opening or the focal lenses has to be changed.

A field size of 1.2×2.3 mm can be obtained based on the maximum homogenizer beam size: 12×23 mm. In ablation, the maximum fluences or energy densities at the target with the 10x reduction lens are kept at values less than 2.5 J/cm^2. This corresponds to a maximum fluence of 0.025 J/cm^2 at the mask. Thus the stainless steel mask can be used without damage. The conventional chrome-on-quartz mask can also be used because the UV grade fused quartz has a transmission rate higher than 90% at a wavelength of 193 nm. During machining, the positioning platform or stage can move in both X and Y directions and rotate in θ-axis as shown in Fig. 2. The Z-axis movement is used for finer focus adjustment. The XY plane is always kept in perpendicular to the laser beam in operation. The workstation enclosure and frame are all mounted on a vibration isolation optical table to reduce vibration coupling between the mask and the sample on the stage set.

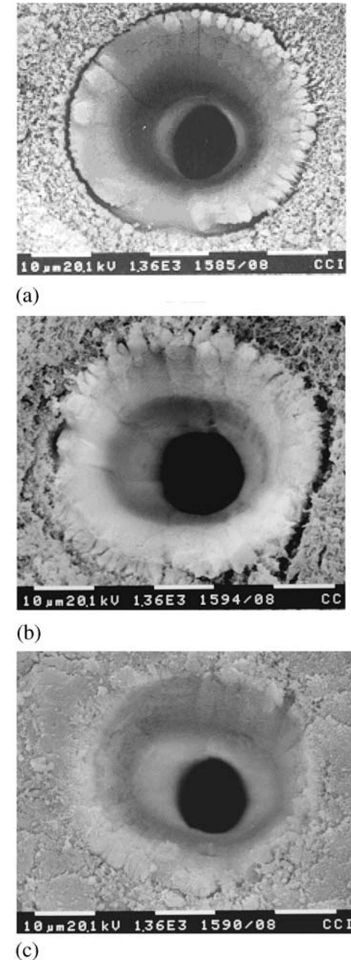

Fig. 3. Effects of repetition rate on surface morphology of glass holes ablated at 2.4 J/cm^2 with 2000 shots (a) 2 Hz, (b) 5 Hz, (c) 10 Hz.

3. Results and discussion

The operating parameters considered in the present experiments include the repetition rate, pulse number, fluence (energy density) and focal plane. The duration of each pulse is fixed at 20 ns. The specific values of the operating parameters can all be preset by a PC-based controller. The material considered is a borosilicate SF-11 glass supplied by Schott North America (www.us.schott.com/sgt/english/products/index.html). SF-11 is one of the most common optical glass having excellent chemical resistance, but has less transmission than that of other popular glass, such as BK7. For a 2-mm thick SF-11, the transmission can be found to be close to zero at a 193-nm wavelength (www.melles-griot.com/products/optics/mp_3_1.htm); as a result, the ArF excimer laser should be extremely effective for ablation of the borosilicate glass. The typical sample size used in the present study is 0.2 mm in thickness and 25 mm^2 in area.

3.1. Single microhole or microwell

The surface morphology for a single hole made by the single opening mask is first studied. Fig. 3 shows the scanning electronic microscope (SEM) micrographs of the ablated holes at three different pulse repetition rates while the fluence and pulse number (number of shots) are kept constant at 2.4 J/cm^2 and 2000, respectively. As shown, the bore diameter is approximately 20 μm. This size is expected since the circular opening on the mask is 200 μm and the circular pattern is printed onto the substrate after a 10x reduction. The SEM images were taken by a Philips Model 515 SEM. Since glass is a dielectric material, a thin gold film ($\sim$10 nm thick) is coated on the ablated glass sample by vacuum evaporation to make it conductive for SEM observation. In order to guarantee laser machining quality, the focal plane has been readjusted according to each sample thickness for perpendicular contact between the laser beam and the sample surface.

For the three pulse repetition rates considered, the lower pulse repetition rate (2 Hz) leads to rougher machined surface and poorer ablating efficiency, while the higher pulse repetition rate (10 Hz) results in more compact material residues and smoother surface. This is consistent with the expectation since at low pulse

repetition rates, the debris or recast from laser ablation have sufficient time to cool down to accumulate into larger debris, resulting in a rougher surface. On the other hand, at high pulse repetition rates, the debris can be bombarded by the subsequent laser pulses and can be ionized into much finer sizes, resulting in smoother surface appearance. Fig. 3 clearly shows that the after-ablated finer debris produced at higher pulse repetition rates are much denser.

The debris are mainly oxide (SiO_2) layers which are often accumulated on the ablated surface. These debris may be removed from the surface by ultrasonic or solvent cleaning, if they do not adhere strongly to the surface. The surface morphology of the ablated holes after a 7 s 10% hydrofluoric acid (HF) etching is shown in Fig. 4 for the pulse repetition rate at 5 and 10 Hz. As compared with the morphology before the etching shown in Fig. 3, the SEM micrographs shown in Fig. 4 indicate that the debris are removed almost 90% for the 5-Hz case, while the debris for the 10-Hz case are discharged near 10%. Again, this suggests that the debris produced at higher repetition rates (10 Hz) are denser and more cohesive, and are not easily eliminated, even with HF etching. It is noteworthy that, if the etching time increases, the dense debris created at high repetition rates can be gradually removed, but the substrate material, glass, may also be damaged concurrently. The morphology of the ablated glass hole before and after HF etching more than 30 s is shown in the AFM (atomic force microscopy) image of Fig. 5. It is clearly shown in the AFM image that some of the glass near the crater is etched out, although the dense debris also disappear.

Moreover, in ablating holes, the cross-section profile of the holes can be tapered off to a point. This is a feature that is inherent to laser drilling occurring in both projection printing and direct writing. Its magnitude is represented by the taper angle which is the angle between the wall of a drilled hole to the normal of the surface. It has also been found that the taper angle slightly decreases as the fluence, pulse number, or repetition rate increases [11]. Similar tapered walls are also observed earlier in ablating glass-based trenches using the slotted mask [10]. Using shorter pulse durations (e.g., ultrafast in femtosecond) or higher numerical apertures, the taper angle for glass-based structures can be reduced to a few degrees only [12,13].

3.2. Machining rate and precision control

The machining or ablation depth of the hole can be measured directly from the SEM micrographs. Based on the images shown in Figs. 3 or 4 and those reported by Tseng, Chen, and Ma [10], a mathematical correlation

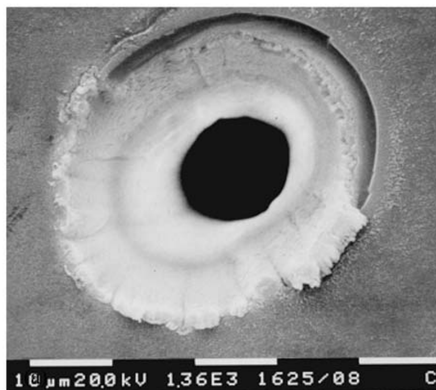

(a)

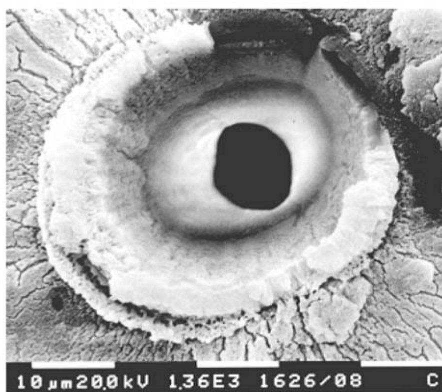

(b)

Fig. 4. SEM images of surface morphology of ablated glass holes after 10% HF etching (a) ablating at 5 Hz, (b) ablating at 10 Hz.

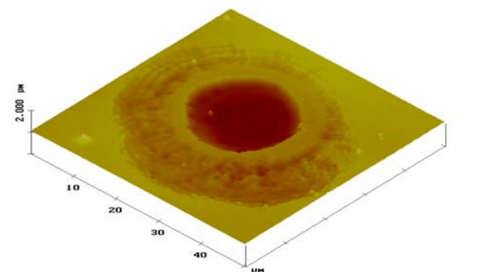

(a)

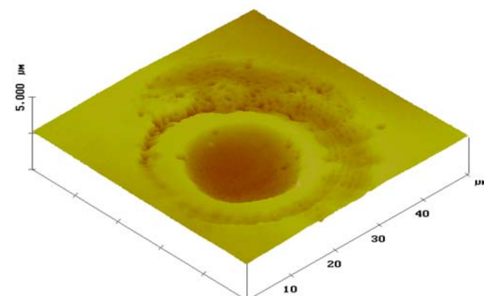

(b)

Fig. 5. Surface morphology of ablated glass hole with and without over (long) HF etching (a) no HF-etching after ablation, (b) over HF-etching after ablation.

between the ablation depth and pulse number can be obtained. In fact, it has been found out that the ablation depth increases linearly with the pulse number, which means that each pulse at a specific fluence contributes equally to the ablation depth

$$d = \Delta d N, \tag{1}$$

where d is the ablation depth in (μm); N is the number of pulses or shots. Here Δd, the ablation depth per pulse or the ablation rate, is normally a function of the fluence and can be determined experimentally. For the fluence at $2.4\ \mathrm{J/cm^2}$, Δd is 0.16 μm. Also, for the present experiment set-up, the effects of the pulse repetition rate on the ablation rate are insignificant for the range considered, i.e., 2–10 Hz, and can be ignored. Consequently, the parameter Δd in (μm) can be further correlated very well with the well-known Beer–Lambert law [8,13]

$$\Delta d = \ln(F_\mathrm{i}/F_\mathrm{t})/\alpha, \tag{2}$$

where α is the absorption coefficient, and F_i and F_t are the incident and threshold fluences, respectively. In addition to the properties of the material to be ablated, the parameters α and F_t should also be a function of the pulse duration. For the present experimental set-up (20-ns pulse duration), the absorption coefficient and threshold fluence for ablating SF-11 glass have been found to be $1.35 \times 10^4\ \mathrm{cm^{-1}}$ at 193-nm wavelength (wavelength of ArF excimer laser) and $0.27\ \mathrm{J/cm^2}$, respectively, which are similar to those reported by Tseng, Chen, and Ma [10].

The correlation between the constants in Eqs. (1) and (2) and the experimental data are extremely consistent. The corresponding correlation coefficients for fitting each constants are all higher than 0.99, which means the ablation depth correlates with the pulse number and fluences almost perfectly. The correlation coefficient is used to gauge the accuracy of correlation and always lies between -1 and $+1$. A value of zero occurs when the two variables are totally independent of each other, while it reaches 1 when the two variables correlate perfectly.

As a result, Eqs. (1) and (2) can be directly used to precisely control the ablation rate and very accurate micromachining operations can be performed. Thus, many applications demanding high precision machining of glass can be developed. Recently, excimer lasers have become powerful tools in making alignment marks for IC masks, microscope reticles, and eyeglass marks, as well as in tailoring optical fibers, optical lenses, and glass molds. The other main advantage is that the use of excimer laser can allow careful processing of these high-precision glass structures without affecting their strength and properties. The procedure in making a glass mold will be illustrated later.

3.3. Comparison with polymer

Fig. 6 shows the SEM micrographs of the surface morphology of the three materials: polyimide, single crystal silicon, and SF-11 glass after ablation at a fluence of $2.4\ \mathrm{J/cm^2}$ and a repetition rate of 5 Hz with 2000 shots. As mentioned earlier, in micromachining, excimer lasers remove the material from a substrate mainly through an ablation mechanism. Ablation can be one or a mix of two processes: ‘‘photothermal’’ and ‘‘photochemical’’. A photochemical or electronic process is often referred to as a non-thermal process because the removal of material is caused by a direct breaking of atomic bonds as energy is absorbed. In contrast, the absorbed laser energy is converted to lattice vibrational energy (thermal) to melt and vaporize the material in a

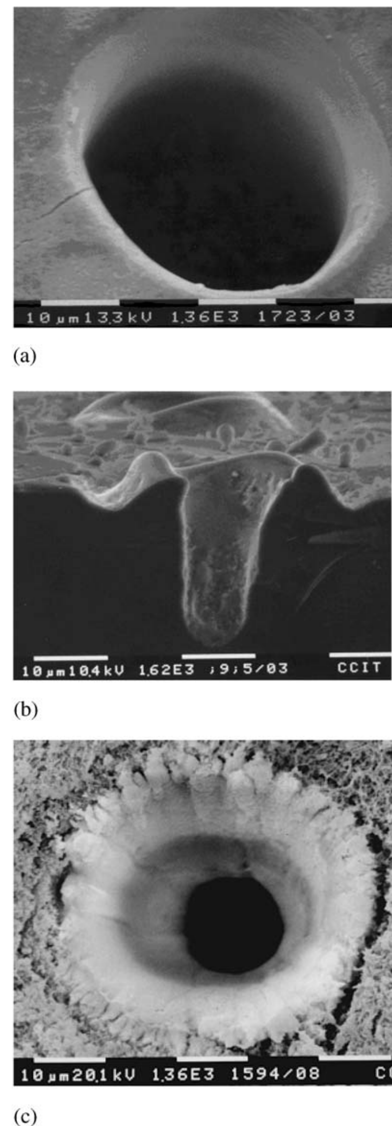

Fig. 6. Surface morphology of three different materials ablated at $2.4\ \mathrm{J/cm^2}$ with 2000 shots (a) polyimide, (b) silicon, (c) borosilicate glass.

photothermal process. To directly break atomic bonding, the intensity of the laser beam should be higher than a threshold value, which is mainly dependant on the material to be ablated and the wavelength of the laser. At intensities below the ablation threshold, the absorbed energy heats the substrate and raises the substrate temperature higher than its boiling or sublimation point. Consequently, the material begins to liberate. Both the photothermal and photochemical processes liberate molecular-sized materials from the surface. The two processes can occur in varying degrees of combination in micromachining that uses high-intensity excimer lasers [8,14]. Normally, the temperature profile resulting from the photochemical process can often produce extensive damage in the heat-affected zone surrounding the melted or vaporized region. On the other hand, in the photochemical process, the pulse duration is far shorter than the thermal diffusion time scale and the ablation depth per pulse is often greater than the optical absorption depth. Thus, the amount of residual energy left in the substrate is typically small. Consequently, the photochemical process is preferred in micromachining.

As shown in Fig. 6a, the surrounding surface of the opening of the polyimide is much more regular and cleaner than that of glass or silicon. Because the polyimides have relatively low ablation threshold and the photochemical process dominates, the photons of the excimer laser has sufficiently high energy (6.42 eV for ArF laser) to directly break the main chain bonds of polyimide and to remove materials by the photochemical process with minimal heat transfer to the surrounding substrate [2]. Also, as shown, the polyimide substrate tends to be free from melting, debris, recasting or other evidence of thermal damage. It has been found the ablation rate for some polymers is also consistent with the Beer–Lambert law, at least for a limited range of fluences above the threshold. Zhang, et al. [15] used a KrF excimer laser (248-nm wavelength) with a 26-ns duration time to ablate a polyimide film under two different annealing conditions. They found that changing the annealing condition had no noticeable effect on the threshold fluence (F_t), which was about 100 mJ/cm^2. However, the absorption coefficients (α) increased from 1.42×10^5 to 2.58×10^5 cm^{-1} by elevating the annealing temperature from 100 to 400°C. The invariance of the threshold fluence by annealing temperature again suggests the photochemical nature of excimer laser-induced ablation of polymides. It is to be noted that polyimides have excellent strength, as well as large thermal and chemical resistances, and have been used in many demanding industrial applications, especially in the electronics industry. Excimer laser has been employed for drilling holes in polyimides used for multilayer and flexible printed circuit boards, tape automated bonding, and ink-jet printer heads [2].

3.4. Comparison with silicon

The photothermal process usually associates with the ablation of glass and silicon, which possess comparatively high thresholds [8,16]. The change in the ablation process greatly affects the surface morphology and the shape or profile of the laser-induced features. Fig. 6b shows the SEM micrograph of the cross-section of an ablated hole in Si. The surface morphology around the crater region and the shape of the hole in Fig. 6b are much different from those of polyimides shown in Fig. 6a. The recast and debris can be clearly seen in the crater region in Fig. 6b, but they are not visible in Fig. 6a. The trace of molten material can be observed in the figure. It suggests that the target material is removed in both vapor and liquid phases, i.e, the photothermal process. The molten materials can be expelled by a recoil pressure during vaporization, also known as the molten-droplet sputtering in ablation [10,17]. The presence of the molten phase can lead to recast or debris creating an unstable ablating process; as a result, recast or debris is considered one of major defects in laser ablation. In general, both debris and recasts are the molten droplets redeposited and solidified on the surface either inside or outside of the crater; debris are accumulated on the surface, while recasts are solidified into the surface layer. However, frequently, these two types of defects are not easy to distinguish.

In ablating silicon, the 'corona' or 'ripple' shape of recast near the crater region are formed and can be seen in Fig. 6b as part of the surface, while, in ablating borosilicate glass, the debris or SiO_2 flakes are condensed around the crater and depicted in Fig. 6c (or Fig. 5a). It is believed that having different solidification time scales is the main reason to cause the molten droplets solidified in different forms. The thermal diffusion length, L_{th}, is approximated to be $(\alpha_t \tau)^{1/2}$, where α_t is the thermal diffusivity and τ is the laser pulse duration. For silicon, the thermal diffusivity is about 93 mm^2/s [18], while for borosilicate glass, α_t is approximately 0.68 mm^2/s [19]. As a result, the L_{th} of silicon is about 12 times of that of glass. In other words, the heat of the molten silicon droplets can be 12 times quicker than that of glass to be transferred to the surrounding silicon near the surface. The heat can quickly melt the silicon surface layer, and the droplets and molten surface layer can be solidified into one undistinguishable surface layer. On the contrary, the heat of the molten glass droplets cannot be transferred fast enough to melt sufficient amount of glass to form an integrated surface layer and, instead, the molten droplets solidify individually to form a flake or single debris. Infact silicon is a metal and two pieces of molten silicon should be easily solidified together. On the other hand, the borosilicate glass is a ceramic and is composed of oxides and many other elements. Also glass does not

have a melting point. All of these properties can cause difficulties for two pieces of molten (or soften) glass to be solidified together.

As shown in Fig. 6, the feature size of the ripple or debris is actually on the same order of magnitude of the ablated hole size. As mentioned earlier, the debris may be removed from the surface by ultrasonic or solvent cleaning, if they do not adhere strongly to the surface. On the other hand, the recasts make the surface irregular or rippling and can only be minimized by reducing the volume of the melt pool created by ablation having higher fluences, shorter pulse durations, and a strong optical absorption.

Recently, the ripple shape of recast and other types of damage have been observed in ablation of silicon using a femtosecond (fs) laser, in spite of the fact that the ultrafast or fs laser machining is often considered 'damage-free', in contrast to ablation with much longer-pulse. Borowiec, et al., [20] found that the amount of the sputtering molten droplets to form the corona increases as the fluence increases, while Bonse, et al. [21] classified the damage morphology into bobbles, columns, and ripples in ablating silicon materials by femotsecond lasers. Furthermore, Bonse, et al. [21] and Jeschke, et al. [22] have studied the ablation threshold of Si using Ti:sapphire fs lasers and found that the threshold fluences of silicon are approximately 0.17 and 0.28 J/cm^2 for pulse durations of 25 and 400 fs, respectively. Bonse et al. [21] also reported that, for laser micromachining of silicon, a pulse of less than 500 fs is not advantageous.

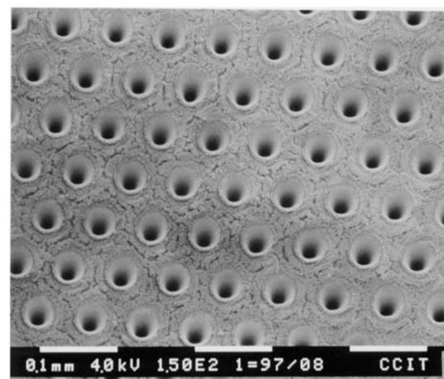

(a)

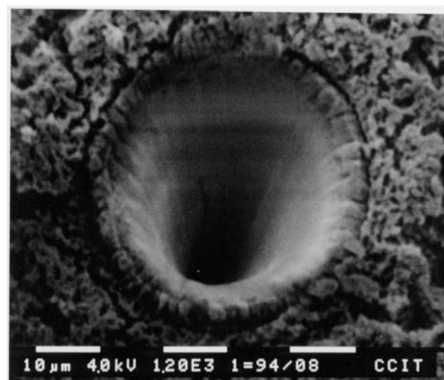

(b)

Fig. 7. Arrays of microholes ablated at 1.2-J/cm^2 fluence, 8000 pulses, and 10 Hz repetition rate (a) array of microholes, (b) enlarged image of microhole.

3.5. Array of microneedles by electroplating

Periodic arrays of microholes can be obtained by controlling the movement of the X–Y stage synchronizing with laser pulse and duration as illustrated in Fig. 2. The same single opening mask used earlier is also adopted in making arrayed microstructures here. Fig. 7 shows an array of microholes fabricated at 1.2-J/cm^2 fluence, 8000 shots, and 10-Hz repetition rate. A close-up view of a hole shown in Fig. 7b reveals that the diameter is close to 35 μm, which is much larger than the laser beam size, 20 μm. This is possibly due to the fact that a humongous amount of heat is accumulated in the entrance region after 8000 shots. The heat melts the region nearby, therefore widening the ablated hole at the entrance.

The tapered microholes made in the glass substrate can be used as a mold for electroplating an array of needle-like metal microprobes. Fig. 8 shows the typical cross-sectional profile of the tapered holes (similar to those depicted in Fig. 7) and the electroplated nickel microneedle. Since glass is a dielectric material, a 4-nm thick gold film is coated on the ablated glass substrate as the seed layer to make it conductive for electroplating. As mentioned earlier, a gold coating is also needed for making an SEM image.

This type of microneedle arrays developed currently can be used for gene and drug delivery [23–25]. Molecules to be delivered either are coated onto the microneedles before insertion into cells or are in solution around the cells when the microneedles are inserted. By carefully controlling the taper angle which can be achieved by shifting the focal plane as illustrated by Chen et al. [7], various shapes of microneedles can be cost-effectively fabricated as compared to those normally made by the expensive silicon-based photolithographic process [23,25].

3.6. Array of microvias

Fig. 9 shows three profiles of microholes made at two different ablation conditions. The one shown in Fig. 9a is the cross-section view of a blind array microholes or microvias with an aspect-ratio (depth to mouth-diameter) on the order of 5. The blind array microvias are ablated at 1.2-J/cm^2 fluence, 8000 shots, and 10-Hz repetition rate, which is similar to that used in making those arrayed holes shown in Fig. 7a. As shown in

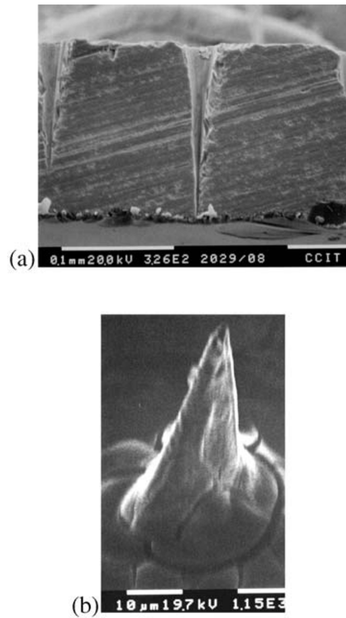

Fig. 8. Profile of microhole and electroplated microneedle (a) profile of microhole fabricated at 1.2-J/cm^2 fluence, 8000 pulses, and 10 Hz repetition rate, (b) electroplated nickel microneedle.

Fig. 9b, through arrayed holes or vias can also be made by increasing the pulse numbers. By carefully examining Fig. 9b, it seems that 'flaps' are formed near the exit of the hole. By increasing the pulse number, the 'flaps' can be eliminated. But at the same time, some materials are chipped off on the exit side. This is a result of fragile materials fracturing out at the exit, which is caused by the acoustic shock of the vaporized material generated by ablation (plasma) rushing out of the hole. This is analogous to the mechanical or press drilling of brittle materials, where pieces breaking out at the exit when there is no backer material.

Also, as indicated in both Fig. 9a and b, materials are not uniformly removed and taper of ablated holes is increased as the hole goes deeper. This is mainly caused by photothermal effects and several factors can be involved. As the holes are ablated deeper or the aspect ratio increases, the internal reflections from the side walls can result in 'waveguiding' and the inability of the molten droplets created by photothermal ablation to escape from the hole increases before the arrival of the next pulse. The enlarged profile on the back or the exit hole side is shown in Fig. 9c to provide the indication that the diameter of the hole on the exit side can be shrunk one order of magnitude smaller. As mentioned earlier, the taper angle for glass-based structures can be reduced by using a shorter pulse duration (e.g., in fs) or a higher numerical aperture.

Recently, forming proper microvias (microholes) becomes increasingly critical in making high-density electronic interconnect and chip packaging devices, because the conventional mechanical drilling technique becomes expensive for vias smaller than 200 μm in diameter due to the frequent breakage of the drill bits and machine downtime [26]. Also, the inability to produce blind vias limits the use of mechanical drilling methods in providing vertical interconnections needed for multi-layer boards.

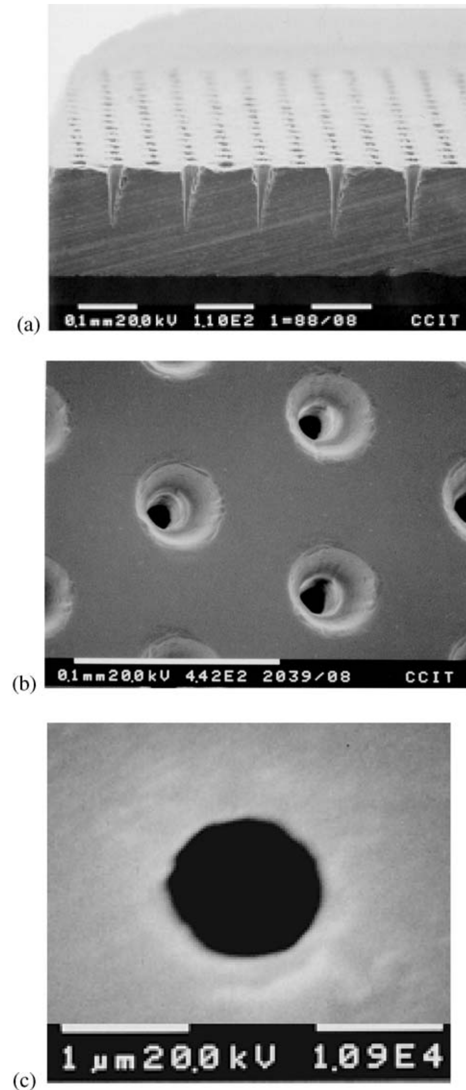

Fig. 9. Profiles of microvias made at two different ablation conditions (a) typical blind microvias, (b) through microvias by increasing the pulse number (c) hole on the exit side.

Laser drilling or ablation has emerged as one of the most feasible technologies for forming microvias. It offers greater resolution over the mechanical technique and is capable of producing vias well below 70 μm [27]. The current results shown in Fig. 9 demonstrate that the projection technique using excimer lasers is capable of drilling blind and through microvias with diameters down to 35 μm with high-precision material removal in glass-based substrates. Also, by using projection techniques with appropriate mask design, many microvias can be drilled simultaneously. For further refining the

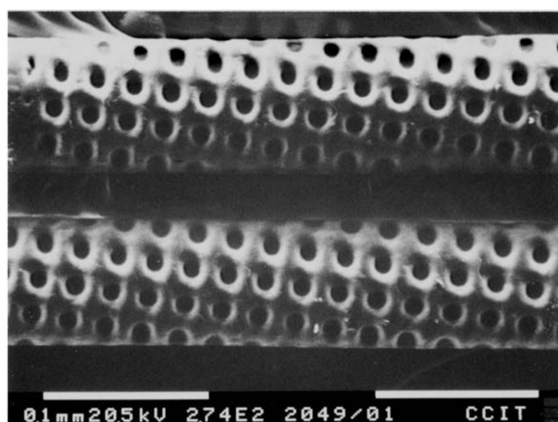

(a)

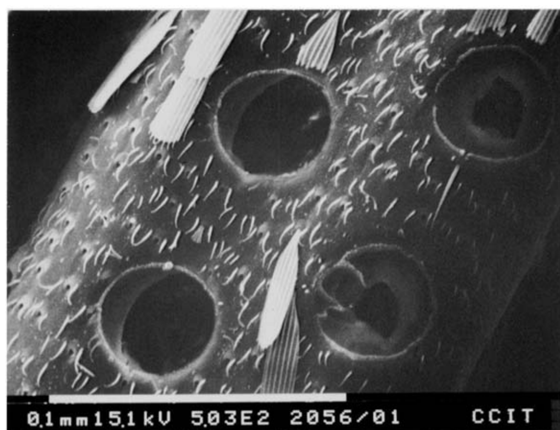

(b)

Fig. 10. Arrays of microholes ablated by ArF excimer laser (a) in human hair (b) in mosquito leg.

laser technique for microvia forming, the impact of laser beam characteristics, ablation conditions, and processing mechanisms, on the profiles of microvias and processing efficiency for different substrates should be investigated.

3.7. Other arrayed microholes

Using the similar technique indicated in the preceding section, many arrayed microholes have been successfully fabricated. For example, Fig. 10a and b show, respectively, an array of microholes ablated at a human hair and a mosquito leg to demonstrate the versatility of the ArF laser used in the present analysis. The diameters of the mask openings used for the human hair and the mosquito are approximately 20 and 40 μm, respectively.

4. Concluding remarks

A technique using a simple mask to provide uniform fluence laser beams for machining single and arrayed microstructures has been developed. Ablation of microholes or microwells in substrates is used to analyze the morphology of ablated structures. The associated threshold fluences and ablation rates are evaluated and discussed. The material considered in the present study is borosilicate glass although ablation of polyimide and silicon are performed and their results are mainly used for comparison. Formations of debris defects in glass and of recast defects in silicon are specifically examined and studied. The reason for forming different types of defects are also presented.

The glass-based arrayed microstructures have been fabricated by repetition ablation through a simple mask. The use of the arrayed microstructures for different applications is discussed. A replication technique to employ the arrayed microstructures for making metal microneedles is specifically demonstrated. Following the procedure developed in the present study, more complex arrayed structures should be able to be fabricated by the repetition technique which, in fact, is similar to the process used to design colorful patterns of cloths by repeating a simple pattern. As a result, the repetition approach can be extremely flexible and cost-effective.

It has been found that glass is an excellent material for laser ablation of single and arrayed microstructures, which are in demand in making a variety of microdevices for photonics and communications industries. A further development in electroplating of metal microprobes from a glass-based mold for bio and medical applications should be encouraged. It is also understood that the development of ablation processes relies on both theory and experiments. A numerical model for simulating the present ablation process should be developed for controlling the process better and for designing the intricate arrayed structures more efficiently.

Furthermore, micromachining of glass-based microstructures becomes increasingly important as the demands for micro-optical and micro-fluidic components are greatly raised. However, micromachining of some special glass-based materials, such as fused silica or quartz is still not appropriate for excimer lasers, because these materials are basically transparent at the wavelength range of excimer lasers. Recently, it has been discovered that, by applying organic solution, including pyrene or chlorine, to the surface, these materials can be ablated by the excimer laser at reasonable ablation rates [28,29]. Further research and development efforts should be committed in this area to enhance the applicability of excimer lasers in micromachining. Finally, since no vacuum or clean-room environment is required during operation and its ability to serve as its own process monitoring, the laser ablation technique developed currently offers an effective and viable alternative to the conventional semiconductor processes.

Acknowledgements

The authors gratefully acknowledge the support of this study by the US National Science Foundation under Grant No. DMI-0002466 and CMS-0115828 and by the ROC National Science Council under Grant No. NSC90-2811-E-002-007. Special thanks also go to Professors Yuan-Fang Chou, Kuang-Chao Fan, Shuo-Hung Chang, and Long-Sun Huang for providing supports and encouragement to the third author (AT), especially, when he was on sabbatical at NTU in 2001. The assistance from Tom C. Fan of Arizona State University in preparing this manuscript should be specifically acknowledged.

References

[1] Endert H, Paetzel R, Basting D. Excimer laser: a new tool for precision micromachining. Opt Quantum Electron 1995;27(12): 1319–35.

[2] Dyer PE. Excimer laser polymer ablation: twenty years on. Appl Phys A 2003;77(2):167–73.

[3] Mendes M, Vilar R. Influence of the working atmosphere on the excimer laser ablation of Al_2O_3-TiC ceramics. Appl Surf Sci 2003;206(1–4):196–208.

[4] Pissadakis S, Reekie L, Hempstead M, Zervas MN, Wilkinson JS. Relief gratings on Er/Yb-Doped borosilicate glasses and waveguides by excimer laser ablation. Appl Surf Sci 2000;153(4): 200–10.

[5] Lee Y-C, Kuo SH. Miniature conical transducer realized by excimer laser micro-machining technique. Sensors and Actuators, A: Phys 2001;93:57–62.

[6] Kancharla VV, Hendricks KK, Chen S. Micromachining of packaging materials for MEMS using lasers. In: Micromachining and Microfabrication Process Technology VII, Proceedings of SPIE, vol. 4557. 2001. Int Society for Optical Engineering, p. 220–4.

[7] Chen YT, Ma KJ, Park JS, Tseng AA. Excimer laser ablation of glass-based arrayed microstructures for optical applications. In: Proceedings of ICALEO 2002, Laser Institute of America, 2002 (published in CD form).

[8] Duley WW. UV Lasers effects and applications in materials science. New York, NY: Cambridge University Press; 1996.

[9] Hansen W, Fuqua P, Livingston F, Huang A, Abraham M, Taylor D, Janson S, Helvajian H. Laser fabrication of glass microstructures. Ind Phys 2002;8(3):18–21.

[10] Tseng AA, Chen YT, Ma KJ. Fabrication of high-aspect-ratio microstructures using excimer lasers. Opt Lasers Eng 2004;41(6): 827–47.

[11] Holmes AS. Laser processes for MEMS manufacture. In: Laser precision microfabrication (LPM 2001). RIKEN Rev. 2002;(43): 63–9.

[12] Schaefer RD. A closer look at laser ablation. Ind Laser Solutions 2000;15(9):21–6.

[13] Pique A, Chrisey DB, Christensen CP. Laser direct-write micromachining. In: Pique A, Chrisey DB, editors. Direct-write technologies for rapid prototyping applications: sensors, electronics, and integrated power sources. San Diego, CA: Academic; 2002. p. 385–414.

[14] Pãtzel R. An introduction to excimer lasers. In: Romaniuk RS, editor. Photonics handbook. 44th ed.. Pittsfield, MA: Laurin Publishing; 2002. p. p247–52.

[15] Zhang X, Grigoropoulos CP, Krajnovich DJ, Tam AC. Excimer laser projection micromachining of polyimide thin films annealed at different temperatures. IEEE Trans Components, Packaging, Manuf Technol C 1996;19(3):201–13.

[16] Laude LD, editors. Excimer Lasers, Dordrecht, Netherlands: Kluwer Academic; 1994.

[17] Chichkov BN, Momma C, Nolte S, von Alvensleben F, Tünnermann A. Femtosecond, picosecond and nanosecond laser ablation of solids. Appl Phys A 1996;63(2):109–15.

[18] Sze SM, editors. Semiconductor sensors. New York NY: Wiley; 1994.

[19] Nikogosyan DN. Properties of optical and laser-related materials a handbook. New York, NY: Wiley; 1997.

[20] Borowiec A, MacKenzie M, Weatherly GC, Haugen HK. Transmission and scanning electron microscopy studies of single femtosecond-laser-pulse ablation of silicon. Appl Phys A 2003;76: 201–7.

[21] Bonse J, Baudach S, Krüger J, Kautek W, Lenzner M. Femtosecond laser ablation of silicon-modification thresholds and morphology. Appl Phys A 2002;74(1):19–25.

[22] Jeschke HO, Garcia ME, Lenzner M, Bonse J, Kruger J, Kautek W. Laser ablation thresholds of silicon for different pulse durations: theory and experiment. Appl Surf Sci 2002;197-198:839–44.

[23] Trimmer W, Ling P, Chin C, Orton P, Gauqler R, Hashmi S, Hashmi G, Brunett B, Reed M. Injection of DNA into plant and animal tissues with micromechanical piercing structures. Proceedings of the IEEE Micro Electro Mechanical Systems (MEMS) 1995; p. 111–5.

[24] Hashmi S, Ling P, Hashmi G, Reed ML, Gaugler R, Trimmer W. Genetic transformation of nematodes using arrays of micromechanical piercing structures. BioTechniques 1995;19(5):766–70.

[25] Reed ML, Clarence W, James K, Watkins S, Vorp DA, et al. Micromechanical devices for intravascular drug delivery. J Pharm Sci 1998;97(11):1387–94.

[26] Zheng HY, Gan E, Lim GC. Investigation of laser via formation technology for the manufacturing of high density substrates. Opt Lasers Eng 2001;36(4):355–71.

[27] Dunsky C. High-speed microvia formation with UV solid-state lasers. Proc IEEE 2002;90(10):1670–80.

[28] Wang J, Niino H, Yabe A. Etching of transparent materials by laser ablation of an organic solutions, in: Laser precision microfabrication (LPM2000). RIKEN Rev 2000;(32):p. 43–6.

[29] Vakanas GP, Tseng AA, Winer P. Laser-assisted chemical etching for embedded microchannels and overhanging microstructures on Si/SiO_2 substrates. J Laser Appl 2002;14(3):185–90.